30
Nonlinear waves

WARNING: unfinished

Wading in the water near a beach and fighting to stay upright in the surf, you are evidently under the influence of a nonlinear dynamics, simply because the breaking waves look so different from the smooth swells at the open sea that gave rise to them. Less apparent but equally nonlinear is the dynamics behind the sonic boom caused by a high-speed airplane passing overhead, the short-range shock wave created by an exploding grenade, or the huge atmospheric shock waves created by thermonuclear explosions. The beauty of fluid mechanics lies in the knowledge that all these effects stem from the same nonlinear aspects of the Navier-Stokes equations.

Any linear dynamics has the powerful property that it permits superposition of solutions to the dynamic equations. A complicated solution to a linear dynamics may in the end be completely resolved into a linear combination of elementary solutions. Leaving the domain of linearity this is no more possible, and solutions take on a more individual character. Typically they are difficult to find and demand special techniques in each particular case. They may also be "nasty", unpredictable and chaotic. Nonlinear phenomena have been at focus in physics for most of the 20'th century, and there is still long way to go.

In this chapter the global laws of balance are first used to analyze large-amplitude shallow-water gravity waves, called *hydraulic jumps*, observed every day in the kitchen sink or on the beach. A similar analysis of large-amplitude waves in an isentropic gas reveals the basic physics behind the *shock waves* created by explosions and by supersonic aircraft. Remarkably, it turns out that the nonlinear dynamic equations governing shallow-water surface waves are similar to the nonlinear equations for large-amplitude waves in an isentropic gas, permitting us to see the analogy between hydraulic jumps and shock waves. Deep-water nonlinear surface waves constitute a clean and elegant problem, although they are much harder to deal with. This chapter owes much to [16, 40, 37, 59].

30.1 Hydraulic jumps

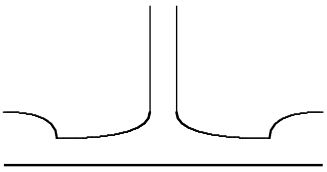

Sketch of the hydraulic jump in a kitchen sink. The water coming down from the tap splays out in a sheet which suddenly thickens.

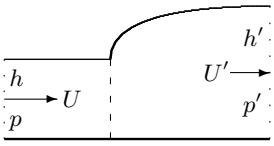

Stationary straight-line hydraulic jump (dashed) of length L (into the paper). Incompressible fluid enters from the left at velocity U and height h and exits on the right at a lower velocity U′ and greater height h′. The entry and exit pressures, p and p′, are hydrostatic. At the front the flow pattern is complicated, often turbulent. The control volume encompasses the whole drawing between the dotted lines.

A stationary *hydraulic jump* or *step* is easily observed in a kitchen sink. The column of water coming down from the tap splays out from the impact region in a roughly circular flow pattern, and at a certain radius the thin sheet of water abruptly thickens and stays thick beyond. The transition region behind the front appears to have a narrow width and contain quite complicated flow. Strongly turbulent stationary hydraulic jumps may also arise in spillways channelling surplus water from a dam into the river downstream.

Stationary jump in planar horizontal flow

We shall begin with an analysis of a stationary jump along a straight line orthogonal to the direction of a uniform flow over a horizontal planar surface. Although stationary jumps like the one in the kitchen sink often have curved fronts, the abruptness of the jump allows us to view it as locally straight in the leading approximation. The flow is assumed to be steady before and after the jump, whereas in the transition region there may be intermittency and turbulence. The Reynolds number is assumed to be so large that viscous friction can be ignored outside the transition region.

Let the liquid stream towards the jump with constant uniform velocity U and constant water level h. Downstream from the jump the flow has a different velocity U' and a different water level h'. The dimensionless *strength* of the jump is defined to be the relative change in height,

$$\sigma = \frac{h' - h}{h} = \frac{h'}{h} - 1 \tag{30-1}$$

Energy balance will later show that the downstream water level must necessarily be the higher, such that the strength is always positive, $\sigma > 0$. A jump is said to be *weak* when $\sigma \ll 1$ and *strong* when $\sigma \gg 1$.

All properties of the jump may, as we shall see, be expressed in terms of the inflow parameters U, h, and the strength σ. Let us choose a control volume with vertical sides containing a stretch of length L of the transition region. The upstream and downstream sides of the control volume are chosen orthogonal to the direction of flow and placed so far away from the transition region that both inflow and outflow are steady and uniform with velocities U and U'. Mass conservation then guarantees that the total mass flux at the outlet is the same as at the inlet,

$$\dot{M} = \rho_0 LhU = \rho_0 Lh'U' \ . \tag{30-2}$$

From this we get the ratio of velocities

$$\frac{U'}{U} = \frac{h}{h'} = \frac{1}{1+\sigma} \ . \tag{30-3}$$

Evidently, the downstream velocity is always the smaller one.

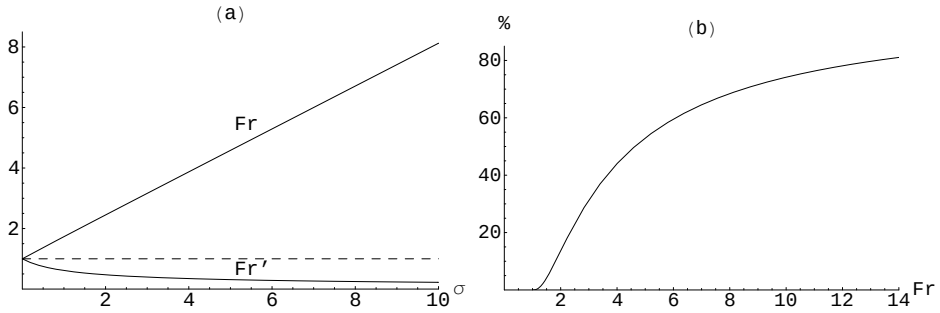

Figure 30.1: **(a)** *The Froude numbers* $\mathsf{Fr} = U/c$ *before and* $\mathsf{Fr}' = U'/c'$ *after the jump, plotted as function of the jump strength* $\sigma = (h' - h)/h$. **(b)** *The percentage of the incoming kinetic energy (30-15) dissipated in the stationary jump as a function of the Froude number.*

Momentum balance (17-14) similarly guarantees that the net outflow of momentum from the control volume equals the total external force acting on the control volume in the direction of the flow. For an inviscid fluid the horizontal force is entirely due to the pressure acting on the two vertical sides of the control volume where the liquid enters or leaves. The pressure in the uniform planar flow that reigns in these regions is hydrostatic, given by $p = p_0 + \rho_0 g_0(h - z)$ at the inlet and $p' = p_0 + \rho_0 g_0(h' - z)$ at the outlet, where p_0 is the constant (atmospheric) pressure on the open liquid surface. Carrying out the force integrals over the inlet and outlet in the usual way, momentum balance becomes,

$$\dot{M}U' - \dot{M}U = \frac{1}{2}\rho_0 g_0 L h^2 - \frac{1}{2}\rho_0 g_0 L h'^2 \ . \tag{30-4}$$

On the left hand side one finds the difference between the momentum fluxes through the outlet and inlet of the control volume, and on the right the difference between the total pressure forces acting on the inlet and the outlet. Eliminating U' and h' using (30-1) and (30-3) the resulting equation may be solved for the entry velocity, to get

$$U = \sqrt{g_0 h}\sqrt{(1+\sigma)(1+\tfrac{1}{2}\sigma)} \ . \tag{30-5}$$

Using again (30-3) we obtain the outlet velocity

$$U' = \sqrt{g_0 h}\sqrt{\frac{1+\frac{1}{2}\sigma}{1+\sigma}} \ . \tag{30-6}$$

The velocity scale in both of these expressions is set by $c = \sqrt{g_0 h}$, which we recognize as the small-amplitude shallow-water wave speed (22-34) in the inflow region. Similarly, the shallow-water wave speed in the outflow region is $c' = \sqrt{g_0 h'} = c\sqrt{1+\sigma}$. Since $\sigma > 0$, it follows immediately that the various velocities obey the inequalities $U > c' > c > U'$. Notice that the smallest outflow velocity is obtained in the strong jump limit, $U' \to c/\sqrt{2}$ for $\sigma \to \infty$.

The dimensionless ratio between the inflow velocity U and the shallow-water wave speed at the inlet is called the *Froude number* (plotted in fig. 30.1a),

$$\mathsf{Fr} = \frac{U}{\sqrt{g_0 h}} = \sqrt{(1+\sigma)(1+\tfrac{1}{2}\sigma)} \; . \tag{30-7}$$

William Froude (1810-79). *English engineer and naval architect. Discovered what is now called scaling laws, allowing predictions of ship performance to be made from studies of much smaller model ships.*

Solving this equation for σ we obtain the strength as a function of the Froude number, *i.e.* of the input values h and U,

$$\sigma = \frac{\sqrt{1+8\mathsf{Fr}^2}-3}{2} \approx \sqrt{2}\,\mathsf{Fr} - \tfrac{3}{2} \; . \tag{30-8}$$

The linear approximation is better than 3.3% for $\mathsf{Fr} > 2$ (problem 30.1). The Froude number at the outlet is similarly defined as

$$\mathsf{Fr}' = \frac{U'}{\sqrt{g_0 h'}} = \frac{\mathsf{Fr}}{(1+\sigma)^{\frac{3}{2}}} = \frac{\sqrt{1+\frac{1}{2}\sigma}}{1+\sigma} \; , \tag{30-9}$$

which is also plotted in fig. 30.1a. Since $\sigma > 0$, we have $\mathsf{Fr} > 1 > \mathsf{Fr}'$, such that the flow is always *supercritical* before the jump, and *subcritical* after.

The jump in the kitchen sink

The nearly circular stationary hydraulic jump in the kitchen sink may be viewed as being locally straight. The position of the jump is difficult to predict because it depends on the shape of the particular kitchen sink (see section 30.1). Here we shall simply place the jump at a certain radius $r = R$ from the center and calculate the shape of the flow before and after.

In accordance with what we did for the planar jump, we shall also here assume that the steady, radial, inviscid flow over the kitchen sink bottom is independent of z, *i.e.* of the form $v_r = u(r)$. Apart from the jump region, the dynamics is governed by the constancy of the mass flux Q and of the Bernoulli function H for a streamline running along the surface,

$$Q = 2\pi r h(r) u(r) \; , \tag{30-10a}$$

$$H = \tfrac{1}{2} u(r)^2 + g_0 h(r) \tag{30-10b}$$

In the general case this becomes a third degree equation for u (or h) with a rather messy solution.

In a typical kitchen sink experiment, as for example the one described below, the jump is usually quite strong with $\sigma \gg 1$. This implies that the local Froude number $\mathsf{Fr}(r) = u(r)/\sqrt{g_0 h(r)}$ will be large in front of the jump and from the constancy of H it follows that $u(r)$ will be nearly constant. Behind the jump the local Froude number will instead be small, which due to the constancy of H implies that the height $h(r)$ will be nearly constant. In terms of the jump values

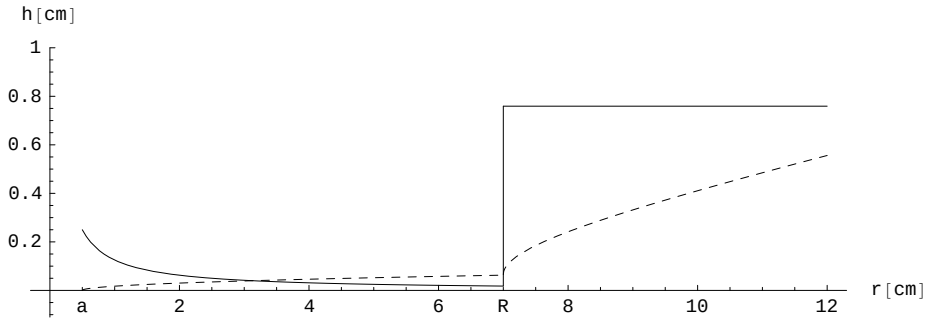

Figure 30.2: *Outline of the hydraulic jump in the kitchen sink discussed in the text and in example 30.1.1. Notice that the height is enlarged by a factor 4 relative to the radius. The fully drawn line is the water level given by the model (30-11) whereas the dashed line is the estimated thickness of the boundary layer. The actual jump is not nearly as sharp as shown here (see section 30.1).*

U and h' we have approximatively,

$$\begin{aligned} u(r) &= U \ , \qquad h(r) = \frac{Q}{2\pi r U} \ , \quad \text{for } r < R \ . \\ u(r) &= \frac{Q}{2\pi r h'} \ , \quad h(r) = h' \ , \qquad \text{for } r > R \ . \end{aligned} \tag{30-11}$$

Notice that because of mass conservation across the jump, $Uh = U'h'$, the Reynolds number $\mathsf{Re} = Uh/\nu = Q/2\pi r\nu$ is continuous and decreases everywhere inversely with the radius. To test whether the assumption of inviscid flow is justified, one may compare the water level $h(r)$ with a thickness estimate of the boundary layer, for example $\delta(r) = 3\sqrt{\nu r/u(r)}$ in front of the jump and $\delta(r) = 3\sqrt{\nu R/U} + 3\sqrt{\nu(r-R)/u(r)}$ behind.

In a kitchen sink experiment it is fairly easy to determine the volume discharge rate Q by collecting water in a standard household measure for a short time. From the radius a of the water jet just before it splays out at the bottom one may determine the average velocity $U = Q/\pi a^2$ which by Bernoulli's theorem should be nearly the same as the radial velocity along the bottom of the sink. From Q, U and R all the jump parameters may then be calculated.

Example 30.1.1 (A kitchen sink experiment): In a home-made kitchen sink experiment (see fig. 30.2) the discharge rate was casually observed to be $Q = 100\ \mathsf{cm}^3/\mathsf{s}$, the radius of the water jet $a = 0.5\ \mathsf{cm}$, and the radius of the jump $R = 7\ \mathsf{cm}$. The velocity before the jump is $U = Q/\pi a^2 = 127\ \mathsf{cm/s}$, and using (30-11) we calculate the height just before the jump to be merely $h = h(R) = Q/2\pi RU = 0.018\ \mathsf{cm}$. The corresponding Froude number is fairly large, $\mathsf{Fr} = U/\sqrt{g_0 h} = 30$, and using (30-8) we determine the jump strength to be $\sigma = 42$. The height after the jump $h' = (1+\sigma)h = 0.76\ \mathsf{cm}$ which is a bit larger than the observed height. The velocity after the jump is $U' = U/(1+\sigma) = 3\ \mathsf{cm/s}$, corresponding to a Froude number of $\mathsf{Fr}' = 0.11$. The Reynolds number at the jump is moderate, $\mathsf{Re} = Uh/\nu = 264$, and the estimated boundary layer thickness at the jump, $\delta(R) = 0.065\ \mathsf{cm}$, is almost four times the water level. Viscosity may thus be assumed to play some role for this experiment, in particular in the region just before the jump, casting the calculation into some doubt.

Energy loss in the stationary jump

It would be tempting to make use of Bernoulli's theorem along a streamline going across the stationary hydraulic jump, but that is impossible because of the unruly fluid in the transition region which messes up streamlines and generates a dissipative (viscous) loss of mechanical energy.

We may nevertheless use mechanical energy balance (17-91) to calculate the rate of loss of energy from the system by keeping track of what mechanical energy goes into the control volume and what comes out. Mechanical energy balance takes the form,

$$\dot{M}\left(\frac{1}{2}U'^2+\frac{1}{2}g_0h'\right)-\dot{M}\left(\frac{1}{2}U^2+\frac{1}{2}g_0h\right)=\frac{1}{2}\rho_0 g_0 L h^2 U-\frac{1}{2}\rho_0 g_0 L h'^2 U'-P\ . \tag{30-12}$$

On the left hand side we have the difference between the rates of outflow and inflow of mechanical energy from the control volume, calculated from the specific mechanical energy density, $\frac{1}{2}\boldsymbol{v}^2+g_0z$, integrated over the outlet and inlet. On the right there is first the difference in rates of work of the pressure forces integrated over the inlet and outlet, and finally P, the rate of loss of energy due to the work of internal friction.

Solving for P we may write,

$$P=\dot{M}\left(\frac{1}{2}U^2+g_0h\right)-\dot{M}\left(\frac{1}{2}U'^2+g_0h'\right)=\dot{M}(H-H') \tag{30-13}$$

where H and H' are the values of the Bernoulli function (16-16) at the surface of the water before and after the jump. This clearly demonstrates that Bernoulli's theorem cannot be fulfilled when P is nonzero. Substituting the downstream quantities using (30-3) we find

$$P=\dot{M}g_0h\ \frac{\sigma^3}{4(1+\sigma)}\ . \tag{30-14}$$

Since the rate of viscous energy loss necessarily must be positive (page 337), we conclude as promised that a stationary hydraulic jump will always have positive strength, $\sigma>0$. Relative to the rate of kinetic energy inflow, $\dot{\mathcal{T}}=\frac{1}{2}\dot{M}U^2$, the *fractional dissipative loss* of kinetic energy becomes (see fig. 30.1b),

$$\boxed{\frac{P}{\dot{\mathcal{T}}}=\frac{\sigma^3}{(1+\sigma)^2(2+\sigma)}\ .} \tag{30-15}$$

It converges as expected to unity for $\sigma\to\infty$. For $\sigma=1$, corresponding to $\mathsf{Fr}=1.73$, only 8.3% of the kinetic energy is lost, whereas for $\sigma=10$ corresponding to $\mathsf{Fr}=8.1$, the fractional loss is 69%. Strong hydraulic jumps are efficient dissipators of kinetic energy, and this is in fact their function in dam spillways where high speed surplus water must be slowed down before it is released into the river downstream of the dam.

Moving hydraulic jumps

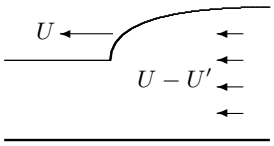

A river bore moving in from the right in water initially at rest. The water behind the front moves slower than the front itself. The velocities are obtained by subtracting U from all the velocities of the stationary jump.

Moving hydraulic jumps are seen on the beach when waves roll in, sometimes in several layers on top of each other. More dramatic *river bores* may be formed by the rising tide near the mouth of a river. When the circumstances are right such waves can roll far up the river with a nearly vertical foaming turbulent front. In the laboratory an ideal river bore can be created in a long canal with water initially at rest. When the wall in one end of the canal is set into motion with constant velocity, a bore will form and move down the canal with constant speed and constant water level.

The only difference between a river bore and a stationary hydraulic jump lies in the frame of reference. The ideal river bore is obtained in the frame where the fluid in front of the jump is at rest. Subtracting U from all velocities (and reversing their directions), the front itself will move with velocity U, and the fluid behind the jump will move in the same direction with velocity $U - U'$, which is smaller than the shallow-water velocity $c' = \sqrt{g_0 h'}$ behind the jump for $\sigma < 2.21$.

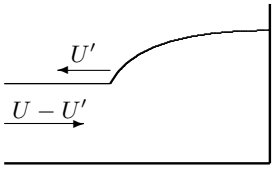

A reflection bore in a closed canal is obtained by subtracting U' from all velocities of the stationary jump.

There is also the possibility of choosing a reference frame in which the fluid behind the jump is at rest. Subtracting U' from the velocities of the stationary jump, this describes a stationary flow being reflected in a closed canal. Such a *reflection bore* moves with velocity U' out of the canal while the flow into the canal has velocity $U - U'$.

> The reflection bore has in fact some bearing on the stationary jump in the kitchen sink. The layer of fluid spreads initially over the bottom of the sink with a high Froude number, and thus a roughly constant velocity and decreasing thickness. The spreading layer of fluid encounters resistance against the free flow from the sides of the sink, or from the slight slope and curvature of its bottom (or even from the increasing viscous friction in the thinning layer of water). This creates a reflection bore with small Froude number, which moves inwards with roughly constant height and increasing velocity, until it stops when it encounters an outflow with velocity and thickness that fits a stationary jump. One may also observe that when the faucet is closed the stationary jump in the kitchen sink immediately turns into a river bore moving towards the center.

Thickness of a hydraulic jump

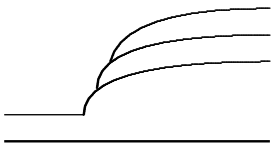

A river bore is "pumped up" by small-amplitude surface waves of sufficiently long wavelength. Short waves move too slowly to catch up with the jump.

A river bore is created by the rising tide at the river mouth, and as long as the tide keeps rising, it will continue to pour more water in. The additional water supplied by the rising tide in a small time interval may be thought of as a small-amplitude surface wave moving upriver on top of the already existing bore. Although this mechanism is most obvious for the river bore, both the reflection bore and the stationary hydraulic jump must also be built up "from behind" by small-amplitude waves.

Any small-amplitude surface wave may be resolved into a superposition of harmonic waves with a spectrum wavelengths. Consider now a harmonic wave with wavelength λ on its way upstream towards a stationary hydraulic jump. In the rest frame of the outflow, the energy in a harmonic wave with wave number

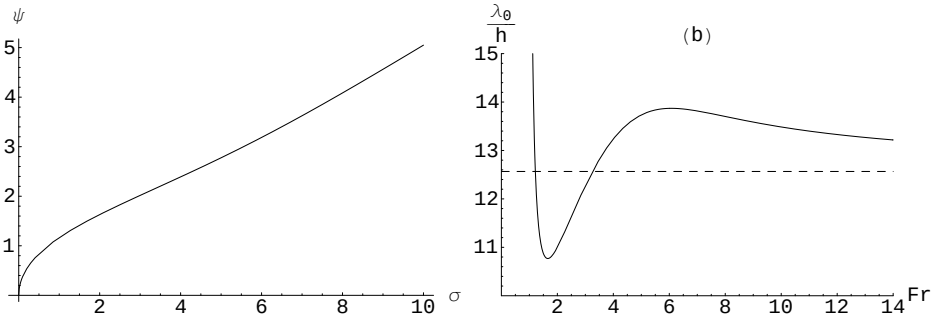

Figure 30.3: **(a)** *The solution $\psi(\sigma)$ to eq. (30-17). For $\sigma \to 0$ the ratio behaves as $\sqrt{\sigma}$, while for $\sigma \to \infty$ it increases as $\sigma/2$.* **(b)** *The ratio λ_0/h of the minimal wavelength in units of the height h before the jump as a function of Froude number Fr. For $\mathsf{Fr} \to \infty$ the ratio becomes constant, $\lambda_0/h \to 4\pi$ (dashed line).*

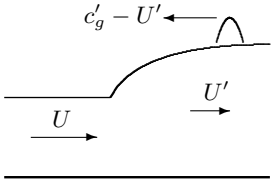

A small-amplitude wavelet moving towards the stationary jump with velocity $c' - U' > 0$.

$k = 2\pi/\lambda$ moves with the group velocity of a gravity wave (22-31). For liquid of depth h' the group velocity becomes,

$$c'_g = \frac{1}{2}\sqrt{\frac{g_0}{k}\tanh kh'}\left(1 + \frac{2kh'}{\sinh 2kh'}\right) \ . \tag{30-16}$$

In the rest frame of the jump, the wave propagates towards the jump with velocity $c'_g - U'$ which must be positive if the wave shall ever reach the jump. Since $c'_g \to \sqrt{g_0 h'}$ for $k \to 0$ and $U' < \sqrt{g_0 h'}$, the condition $c'_g > U'$ may always be fulfilled provided the wave number k is sufficiently small, *i.e.* the wavelength exceeds a certain minimum value, $\lambda > \lambda_0$. The minimal wavelength λ_0 is found by solving the equation $c'_g = U'$, which after division by $\sqrt{g_0 h'}$ takes the form,

$$\frac{1}{2}\sqrt{\frac{\tanh\psi}{\psi}}\left(1 + \frac{2\psi}{\sinh 2\psi}\right) = \mathsf{Fr}' = \frac{\sqrt{1+\frac{1}{2}\sigma}}{1+\sigma} \ , \tag{30-17}$$

where $\psi = kh' = 2\pi h'/\lambda_0$. This transcendental equation may be solved for ψ and the result is shown in fig. 30.3a as a function of the jump strength σ. In fig. 30.3b this is converted to a plot of the ratio λ_0/h of the minimal wavelength to the *upstream* height h as a function of the Froude number Fr.

A small-amplitude gravity wave moving upstream towards the jump must have wavelength greater than λ_0. Its front cannot be sharper than that.

The hydraulic jump acts effectively as a high-pass filter on wavelengths, only letting waves with sufficiently large wavelength, $\lambda > \lambda_0$, through to "feed" it. The smooth part of a hydraulic jump cannot contain details much smaller than the waves that maintain it, so the minimal wavelength λ_0 may be used as a measure of the thickness of the transition region behind the front. At the front itself, shorter wavelengths may be generated by the chaotic motion and turbulence, thereby creating undulations in the otherwise smooth transition region.

Example 30.1.2: A river bore with front height $h' - h = 1$ m moves up a river of depth $h = 0.5$ m. The jump strength is $\sigma = (h' - h)/h = 2$, corresponding to $\mathsf{Fr} = 2.45$, and the front velocity becomes $U = 5.4$ m/s while the velocity of the flow behind the front is $U - U' = 3.6$ m/s. From fig. 30.3b we find $\lambda_0/h = 11.6$, so that the minimal wavelength and thus the thickness becomes $\lambda_0 = 6.7$ m.

30.2 Normal shocks in ideal gases

An explosion in a fluid at rest creates an expanding fireball of hot gases and debris which pushes the fluid in front of it. If the velocity imparted to the fluid by the explosion is smaller than the velocity of sound in the fluid, a sound wave will run ahead of the debris and with a loud bang inform you that the explosion took place. If on the other hand the initial expansion velocity of the fireball is larger than the sound velocity in the fluid, the first sign of the explosion will be the arrival of a supersonic front (here we disregard the flash of light which may arrive much earlier). The sudden jump in the properties of a fluid at the passage of a supersonic front is called a *shock*. Stationary shocks may arise downstream from a constriction in a duct where the flow under suitable conditions discussed in section 16.4 will be supersonic. The understanding of shocks is of great importance for the design of supersonic aircraft, and of jet and rocket engines.

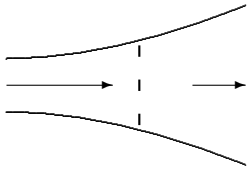

A stationary shock (dashed) in an expanding nozzle. The inflow is supersonic and the outflow subsonic.

Stationary planar normal shocks

We shall begin by analyzing stationary planar shocks, which like plane waves are normal to the direction of the flow. We shall later see that shocks are in fact not much thicker than the molecular length scale, allowing us to view all shocks as singular and locally planar. In the rest system of the shock we choose a narrow control volume just containing an area A of the shock front. Upstream from the shock the gas has velocity U, temperature T, pressure p, and density ρ; downstream it has velocity U', temperature T', pressure p', and density ρ'.

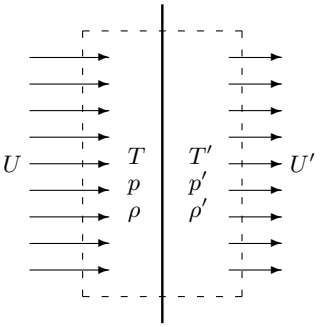

A piece of a stationary normal shock front. Fluid comes in from the left with supersonic velocity U, temperature T, pressure p and density ρ. The fluid emerges on the right with subsonic velocity U'.

There is a strong analogy between a hydraulic jump and a shock. The *strength* of the shock is however defined as the relative pressure increase,

$$\sigma = \frac{p' - p}{p} = \frac{p'}{p} - 1 \ . \tag{30-18}$$

We shall see below that the Second Law of Thermodynamics requires that $\sigma > 0$. A shock is said to be *weak* when $\sigma \ll 1$ and *strong* when $\sigma \gg 1$.

Since the shock is so narrow there will be essentially no room for dissipation of energy, allowing us to apply Bernoulli's theorem. Using the pressure function (16-32) for an ideal gas with adiabatic index γ, we obtain three basic equations, called the *Rankine-Hugoniot* relations,

$$\rho U = \rho' U' \ , \tag{30-19a}$$

$$\rho U^2 + p = \rho' U'^2 + p' \ , \tag{30-19b}$$

$$\frac{1}{2}U^2 + \frac{\gamma}{\gamma - 1}\frac{p}{\rho} = \frac{1}{2}U'^2 + \frac{\gamma}{\gamma - 1}\frac{p'}{\rho'} \ . \tag{30-19c}$$

Pierre Henri Hugoniot (1851-1887). *French engineer.*

These relations are simple rearrangements of mass, momentum, and energy balance across the shock. They may be solved explicitly for the downstream parameters in terms of the upstream ones (see problem 30.3), but it is much more convenient to express the solution in terms of the strength of the shock.

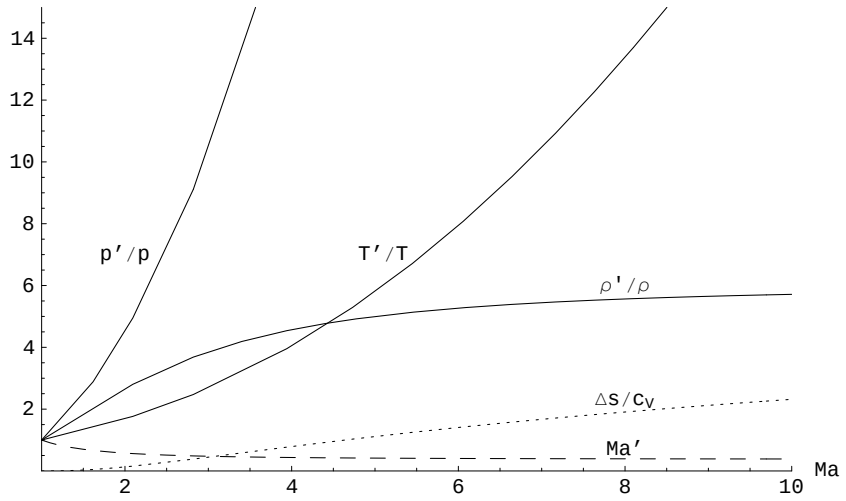

Figure 30.4: *The dimensionless Rankine-Hugoniot parameters as function of the inflow Mach number for $\gamma = 7/5$. The fully drawn curves are the ratios of pressure, density, and temperature. The dashed curves is the outflow Mach number Ma', and the dotted curve is the specific entropy jump at the shock, $\Delta s/c_V$ given in (30-24).*

Using (30-19a) to eliminate U' in (30-19b), we obtain,

$$U^2 = \frac{\rho'}{\rho} \cdot \frac{p' - p}{\rho' - \rho} \,, \qquad\qquad U'^2 = \frac{\rho}{\rho'} \cdot \frac{p' - p}{\rho' - \rho} \,, \tag{30-20}$$

where the second equation is obtained fromt the first by swapping primed and unprimed variables. Inserting this into (30-19c) we find the ratio of densities,

$$\frac{\rho'}{\rho} = \frac{\gamma(p + p') + p' - p}{\gamma(p + p') - p' + p} \,. \tag{30-21}$$

Expressing the right hand side in terms of the strength we find

$$\frac{\rho'}{\rho} = \frac{U}{U'} = \frac{2\gamma + (\gamma + 1)\sigma}{2\gamma + (\gamma - 1)\sigma} \,. \tag{30-22}$$

The temperature ratio may now be obtained from the ideal gas law, $T'/T = (p'/\rho')/(p/\rho)$.

Since we are interested in supersonic flow, it is most convenient to express the velocities in terms of the dimensionless Mach numbers, $\mathsf{Ma} = U/c$ and $\mathsf{Ma}' = U'/c'$, where $c = \sqrt{\gamma p/\rho}$ and $c' = \sqrt{\gamma p'/\rho'}$ are the sound velocities before and after the shock. Using (30-20) we find,

$$\mathsf{Ma} = \sqrt{1 + \frac{\gamma + 1}{2\gamma}\sigma} \,, \qquad\qquad \mathsf{Ma}' = \sqrt{1 - \frac{\gamma + 1}{2\gamma}\frac{\sigma}{1 + \sigma}} \,. \tag{30-23}$$

Here the second equation is obtained from the first by swapping primed and unprimed variables, which according to the definition (30-18) amounts to replacing σ by $-\sigma/(1 + \sigma)$.

Up to this point, the strength may in principle range over both negative and positive values in the interval $-1 < \sigma < \infty$. The physical asymmetry between positive and negative strength becomes apparent when we calculate the change in specific entropy $\Delta s = s' - s$ across the shock. Using (D-21c) we find,

$$\frac{\Delta s}{c_V} = \log\left[\frac{p'}{p}\left(\frac{\rho'}{\rho}\right)^{-\gamma}\right] = \log(1+\sigma) - \gamma \log\frac{2\gamma + (\gamma+1)\sigma}{2\gamma + (\gamma-1)\sigma}\ , \qquad (30\text{-}24)$$

where c_V is the specific heat constant of the gas (D-18). The right hand side is a monotonically increasing function of σ which vanishes for $\sigma = 0$ (see problem 30.4 and fig. 30.4). But by the Second Law the specific entropy is not permitted to decrease across the shock, and consequently we must require that σ be positive. We have thus reached the promised conclusion that *in a stationary shock the velocity must go from supersonic (*$\mathsf{Ma} > 1$*) to subsonic (*$\mathsf{Ma}' < 1$*) in the downstream direction.* The various dimensionless quantities are plotted in fig. 30.4 as functions of the inflow Mach number Ma.

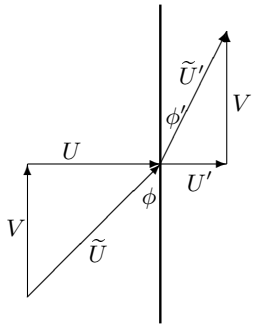

Geometry of an oblique stationary shock in a reference frame moving tangentially with velocity V. The flow velocities in the moving frame are $\widetilde{U}$ and $\widetilde{U}'$ with angles of incidence ϕ and ϕ'.

Oblique shock

An *oblique* planar shock front may be obtained in a reference frame moving tangentially to the stationary normal shock with constant velocity V. In the moving frame the flow velocities are denoted $\widetilde{U}$ and $\widetilde{U}'$ with angles of incidence ϕ and ϕ'. Using that the tangential velocity is the same on both sides of the shock, $V = U\cot\phi = U'\cot\phi'$, we obtain a relation between incidence and strength,

$$\boxed{\frac{\tan\phi'}{\tan\phi} = \frac{U'}{U} = \frac{2\gamma + (\gamma-1)\sigma}{2\gamma + (\gamma+1)\sigma}\ .} \qquad (30\text{-}25)$$

Expanding this relation for $\sigma \ll 1$ allows us to calculate the *deflection angle* $\phi - \phi'$ for a weak shock,

$$\phi - \phi' \approx \frac{\sin 2\phi}{2\gamma}\sigma\ . \qquad (30\text{-}26)$$

The deflection angle is small and positive in this limit.

The angle of incidence is always given by $\sin\phi = U/\widetilde{U}$, and since $U \to c$ for $\sigma \to 0$, the incidence angle for a weak oblique shock equals the *Mach angle*,

$$\boxed{\phi_0 = \arcsin\frac{1}{\widetilde{\mathsf{Ma}}}\ ,} \qquad (30\text{-}27)$$

where $\widetilde{\mathsf{Ma}} = \widetilde{U}/c$ is the Mach number of the inflow. What we perceive as a *sonic boom* is a weak shock cone with half opening angle ϕ_0 trailing a supersonic aircraft. A simple geometric construction due to Mach permits us to view the cone as the envelope of all the spherical sound waves emitted earlier from the nose of the aircraft.

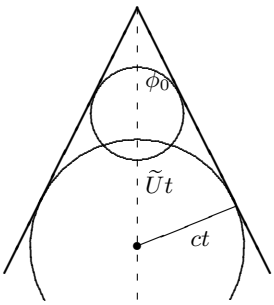

The Mach construction of the shock cone for a supersonic object. In a time t, the object moves forward a distance $\widetilde{U}t$ while the sound emitted at $t = 0$ forms a sphere of radius ct. The opening angle of the envelope of all spheres is $\sin\phi_0 = ct/\widetilde{U}t = c/\widetilde{U} = 1/\widetilde{\mathsf{Ma}}$.

Example 30.2.1: For an aircraft at $\widetilde{\mathsf{Ma}} = 2$, the Mach angle is 30°, so when you hear the sonic boom of the aircraft flying at 20 km altitude, it is already $20\sqrt{3} \approx 35$ km beyond your position.

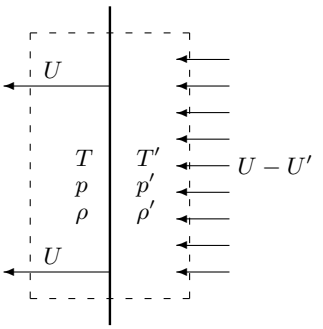

A planar shock moving towards the left with supersonic velocity U into a gas at rest. The fluid behind the front moves to the left with velocity $U - U'$ which may or may not be supersonic.

Moving normal shock

A stationary planar normal shock may be converted to a normal shock moving through a gas at rest by choosing a reference frame moving with velocity U. In this frame, the previously incoming gas will now be at rest, whereas the shock front itself moves in the opposite direction with velocity U, and the gas behind the front moves in the same direction with velocity $U - U'$ which may or may not be supersonic. Locally, this describes a blast wave arising from a violent explosion, to be discussed in the following section.

Front thickness

Since the gas is completely at rest before the passage of the moving front, it is clear that a moving shock must be "fed from behind", like a hydraulic jump, but because air is non-dispersive all small-amplitude waves move upstream at the same speed, $c' = \sqrt{\gamma p'/\rho'}$. Thus there will be no lower limit to the wavelength of disturbances running upstream towards the front, and from a macroscopic point of view the shock front has vanishing thickness, as long as viscosity can be disregarded.

The only quantity with the dimension of length that may naturally be constructed from the front velocity U and the kinematic viscosity ν is,

$$\delta \sim \frac{\nu}{U} \ . \tag{30-28}$$

For a weak shock in the atmosphere under normal conditions we have $\nu \approx 1.6 \times 10^{-5}$ m^2/s and $U \approx c \approx 340$ m/s, leading to $\delta \sim 44$ nm, so that the viscous thickness of the front is comparable to the mean free path in the gas. This conclusion actually invalidates the calculation, but for all practical purposes a shock front may be assumed to have zero thickness.

Strong shock limit

In the limit of large shock strength $\sigma \gg 1$, the density ratio ρ'/ρ, the velocity ratio U'/U, the ratio $p'/\rho U^2$, and Ma' all approach constant values,

$$\frac{\rho'}{\rho} = \frac{U}{U'} \to \frac{\gamma+1}{\gamma-1} \ , \qquad \frac{p'}{\rho U^2} \to \frac{2}{\gamma+1}, \qquad \mathsf{Ma}' \to \sqrt{\frac{\gamma-1}{2\gamma}} \ . \tag{30-29}$$

For a diatomic gas with $\gamma = 7/5$ we find $\rho'/\rho \to 6$ and $\mathsf{Ma}' \to 1/\sqrt{7} \approx 0.38$. The actual Mach number of the flow behind a moving shock in a stationary gas is $(U - U')/c' \to 1/\sqrt{2\gamma(\gamma-1)}$ which becomes $5/2\sqrt{7} \approx 0.94$ for $\gamma = 7/5$. The flow behind the front is only marginally subsonic in a diatomic gas, whereas in a multi-atomic gas with $\gamma = 4/3$ the flow is marginally supersonic.

30.3 Atmospheric blast wave

A large explosion in the atmosphere generates a *blast wave* bounded by a spherical supersonic shock front. Mostly such blast waves are invisible, but films of nuclear or thermonuclear bomb explosions show that the physical conditions can become so extreme that the blast wave can be seen as a rapidly expanding spherical fireball, appearing right after the initial flash but before the mushroom cloud erupts. In this section we shall investigate the time evolution of such blast waves in the atmosphere, following the road laid out by G. I. Taylor in the 1940's[1].

Radius of the strong shock front

Let the atmosphere initially be at rest with density ρ_0 and pressure p_0. The blast deposits almost instantly a huge amount of energy E_0 within a tiny region of radius a, which initially contains the possibly ionized gases produced in the blast, as well as the solid remains of the bomb if any. The huge pressure in the initial fireball creates a shock front expanding at supersonic speed. After some time t, the shock front has become nearly spherical with a radius $R(t)$ that is very large compared to the initial size a. The volume inside the front contains essentially all of the initial energy E_0 in the form of "shocked" air with only little contamination from the bomb itself. At this stage the shock has become a purely atmospheric phenomenon and all details about its origin in any particular explosion have been "forgotten".

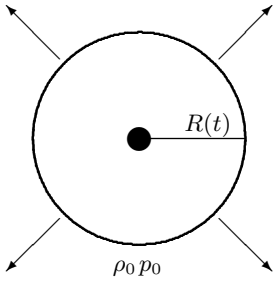

A spherical shock front in the atmosphere some time t after the detonation of a bomb (black circle). Its current radius is $R(t)$, which is much larger than the initial blast region. The atmosphere is at rest with density ρ_0 and pressure p_0. The volume of the sphere consists almost entirely of air.

Under these conditions the radius of the shock front $R(t)$ will be determined by the equations of gas dynamics, and can only depend on time t, the total energy E_0, and the atmospheric parameters ρ_0 and p_0. In a strong shock the ambient pressure p_0 is negligible compared to the pressures inside, implying that $R(t)$ should be finite in the limit of $p_0 \to 0$, and thus only depend on t, E_0, and ρ_0. Since E_0/ρ_0 is measured in units of of $\mathsf{J}/(\mathsf{kg}/\mathsf{m}^3) = \mathsf{m}^5/\mathsf{s}^2$, the only possible form of the relationship is

$$\boxed{R(t) = A\left(\frac{E_0 t^2}{\rho_0}\right)^{1/5}}, \qquad (30\text{-}30)$$

where A is a numerical constant which as we shall see below is very close to unity.

It is remarkable that a phenomenon as violent as an atomic explosion can be contained in such a simple relationship. Taylor used it in 1947 to estimate the yield of the first nuclear bomb to be about 10^{14} J from a time-lapse sequence of photographs in Life Magazine, a feat which is said to have created some embarrassment with the security authorities.

[1]G. I. Taylor, *The formation of a blast wave by a very intense explosion (I. Theoretical discussion, II. The atomic explosion of 1945)*, Proc. Roy. Soc. **A201**, 159-186 (1950). Taylor actually formulated the theory in 1941, but first published it in 1950. Photographs of the first atomic test were declassified by the US Atomic Energy Commission in 1947, although its yield remained classified.

Physical parameters in the strong shock limit

In the strong shock limit we may use the strong shock results (30-29) to determine the physical quantities just inside the front,

$$\frac{\rho_1}{\rho_0} = \frac{\gamma+1}{\gamma-1} \;, \qquad \frac{v_1}{U} = \frac{2}{\gamma+1} \;, \qquad \frac{p_1}{\rho_0 U^2} = \frac{2}{\gamma+1} \;, \tag{30-31}$$

where $U = dR/dt = \frac{2}{5}R/t$ is the shock front velocity and $v_1 = U - U' = (1 - U'/U)U$ is the radial flow velocity just behind the front. The temperature is obtained from the ideal gas law,

$$T_1 = \frac{p_1}{\rho_1}\frac{M_{\mathsf{mol}}}{R_{\mathsf{mol}}} = \frac{2(\gamma-1)}{(\gamma+1)^2}\frac{M_{\mathsf{mol}}U^2}{R_{\mathsf{mol}}} \;. \tag{30-32}$$

where R_{mol} is the molar gas constant and M_{mol} is the molar weight of the gas. Notice that none of these quantities depend on the ambient pressure p_0. In the following we shall use the value $\gamma = 7/5$ for diatomic gas, although the violent initial shock may dissociate a fraction the molecules.

Example 30.3.1 (Trinity): The first atomic bomb test, codenamed *Trinity*, was carried out at Alamogordo, New Mexico on July 16 1945. Its yield was $E_0 \approx 10^{14}$ J which is roughly equivalent to 20,000 tons of the high explosive TNT. Taking $A = 1$ and $\gamma = 7/5$ we find that after $t = 10$ ms the fireball has obtained a radius of $R = 100$ m with the front moving at a speed of $U = 3900$ m/s. The pressure just inside the front is $p_1 = 147$ atm, the density $\rho_1 = 7.2$ kg/m^3, and the temperature $T_1 = 7200$ K, which is comparable to the temperature at the surface of the Sun.

Isentropic radial gas dynamics

A spherically invariant isentropic flow in an ideal gas is described by a purely radial velocity field $\boldsymbol{v} = v(r,t)\boldsymbol{e}_r$, a density field $\rho(r,t)$, a pressure field $p(r,t)$ and the field of specific entropy $s = c_V \log(p\rho^{-\gamma})$. In the absence of gravity and viscosity, the fields obey the dynamic equations,

$$\frac{\partial v}{\partial t} + v\frac{\partial v}{\partial r} = -\frac{1}{\rho}\frac{\partial p}{\partial r} \;, \tag{30-33a}$$

$$\frac{\partial \rho}{\partial t} + \frac{1}{r^2}\frac{\partial\left(r^2\rho v\right)}{\partial r} = 0 \;, \tag{30-33b}$$

$$\frac{\partial s}{\partial t} + v\frac{\partial s}{\partial r} = 0 \;. \tag{30-33c}$$

The first is the Euler equation, the second the continuity equation on radial form, and the last expresses that the flow is isentropic, meaning that the specific entropy is constant along a comoving (particle) orbit. The last equation also shows that if the initial state is *homentropic* with spatially constant specific entropy $\partial s/\partial r = 0$, it will remain so forever. In a strong blast entropy is only produced right at the front, and that does not, as we shall see, lead to a homentropic state.

Strong self-similar shock

In the strong shock limit limit, $p_0 \to 0$, the only parameter with dimension of length is the radius of the shock front $R(t)$, which we for a moment pretend not to know explicitly. The proper non-dimensional radial variable for all the fields is therefore,

$$\xi = \frac{r}{R(t)} \ . \tag{30-34}$$

Including suitable dimensional coefficients depending only on $R(t)$ and ρ_0, the fields are assumed to be of the form,

$$v = \dot{R}(t) u(\xi) \ , \tag{30-35a}$$
$$\rho = \rho_0 \, f(\xi) \ , \tag{30-35b}$$
$$p = \rho_0 \dot{R}(t)^2 q(\xi) \ , \tag{30-35c}$$

where a dot indicates differentiation after time. With this assumption, the spatial variation of the fields is self-similar at all times.

Inserting these fields into the equations of motion (30-33) we obtain three coupled ordinary first order differential equations, and using a prime to denote differentiation after ξ, we find

$$\alpha u + (u - \xi) u' = -\frac{q'}{f} \ , \tag{30-36a}$$
$$(u - \xi) f' = -f u' - \frac{2uf}{\xi} \ , \tag{30-36b}$$
$$2\alpha + (u - \xi) \left(\frac{q'}{q} - \gamma \frac{f'}{f} \right) = 0 \ . \tag{30-36c}$$

where

$$\alpha = \frac{R\ddot{R}}{\dot{R}^2} \ . \tag{30-37}$$

The α-terms on the left-hand side of (30-36) stem from the explicitly time-dependent prefactors of the fields. Since α only depends on t and the other functions only on ξ, it follows from these equations that α must be a constant, independent of time. The solution to (30-37) is then a power law

$$R(t) \sim t^{1/(1-\alpha)} \ . \tag{30-38}$$

The value of α cannot be determined from the dynamic equations alone but depends on the boundary conditions imposed on the solution, in particular the condition that the radial velocity u must vanish at $\xi = 0$. We shall determine it below by requiring the excess energy E_0 to be constant.

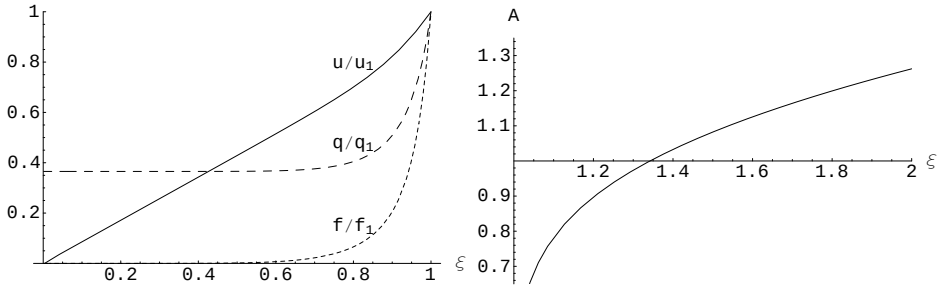

Figure 30.5: **(a)** *The numeric solution to the dynamic equations (30-36) for* $\gamma = 7/5$. *All quantities are normalized to their maximal values at* $\xi = 1$. **(b)** *The dimensionless coefficients A in the blast radius (30-30).*

Numerical solution

The three ordinary first-order differential equations (30-36) need three boundary conditions which may be determined at $\xi = 1$ from the strong shock properties (30-31),

$$f_1 = \frac{\gamma+1}{\gamma-1} \ , \qquad u_1 = \frac{2}{\gamma+1} \ , \qquad q_1 = \frac{2}{\gamma+1} \ . \tag{30-39}$$

Although it is possible to find an analytic solution [68], it turns out to be quite complicated, and it is much easier to integrate the differential equations numerically. The numeric solution is plotted in 30.5a for $\gamma = 7/5$ with the functions normalized by their values at $\xi = 1$. Evidently there are two distinct regions in a strong shock, a *core* for $\xi < 0.7$ where the pressure is nearly constant with $q_0/q_1 \approx 0.37$ and the velocity increases linearly, and a *shell* for $\xi > 0.7$ where the velocity and pressure rise rapidly to meet the required values at the front.

Excess energy

The total energy of the gas in the volume inside the shock front consists of the kinetic energy of the moving gas plus its internal energy. Subtracting the internal energy of the gas before the explosion we find from (17-97) on page 323 the excess of energy inside the shock front,

$$E_0 = \int_0^{R(t)} \left(\frac{1}{2}\rho(r,t)v(r,t)^2 + \frac{p(r,t)-p_0}{\gamma-1} \right) 4\pi r^2 \, dr \ . \tag{30-40}$$

Barring radiative losses, this energy must be constant and equal to the extra energy added to the atmosphere in the point-like explosion. It takes quite a bit of algebraic work to demonstrate explicitly from the dynamics (30-33) and the strong shock properties (30-31) that the time derivative of this expression indeed vanishes.

Inserting the self-similar fields (30-35), the excess energy (30-40) becomes in the limit of $p_0 \to 0$,

$$E_0 = \rho_0 R^3 \dot{R}^2 K(\gamma) \ , \tag{30-41}$$

where $K(\gamma)$ is the integral,

$$K(\gamma) = 4\pi \int_0^1 \left(\frac{1}{2} f(\xi) u(\xi)^2 + \frac{q(\xi)}{\gamma - 1} \right) \xi^2 \, d\xi \ . \tag{30-42}$$

It is immediately clear that for the power law (30-38) to lead to a constant energy, it must have exponent $\alpha = -3/2$, and thus $R \sim t^{2/5}$. This confirms the dimensional analysis (30-30), and inserting $\dot{R} = \frac{2}{5} R/t$ in (30-40) we also obtain an expression for the dimensionless constant,

$$A = \left(\frac{4}{25} K(\gamma) \right)^{-1/5} \ . \tag{30-43}$$

In fig. 30.5b the numeric solution is plotted for a range of γ values. For $\gamma = 7/5$ we have $A = 1.03$, which justifies taking $A \approx 1$ in our earlier estimates.

The weakening shock

As the shock front expands, it decreases in strength until it no more satisfies the conditions for the strong shock approximation used above. The characteristic strength for the breakdown of the strong shock approximation may be chosen to be $\sigma_s = 2\gamma/(\gamma - 1)$ where the two terms in the denominator of the density ratio (30-22) become equal. For $\gamma = 7/5$ we have $\sigma_s = 7$ and thus $p_1 = (1 + \sigma_s) p_0 = 8$ atm. Using the strong shock formalism in the Trinity example 30.3.1 this is estimated to happen at time $t = 119$ ms when the front radius is $R = 268$ m.

Continuing the expansion beyond this point, the core pressure will decrease until it reaches the ambient pressure p_0. At this point the core can no more perform work on the surrounding atmosphere and will stop expanding. The core is very hot due to its large entropy with a correspondingly low density, and the buoyancy of the low-density core will make it rise like a thermal bubble, creating thereby the well-known mushroom cloud. We may estimate the time when the core expansion ceases by equating the core pressure $p = \rho_0 U^2 q_0$ with atmospheric pressure p_0. This is probably a rather bad approximation, but in lieu of a better we find in the Trinity example 30.3.1 that it happens at time $t = 276$ ms when the front radius is $R = 364$ m.

After this point the shock wave continues as spherical wave in the form of a thin shell. When such a front passes a given point, mass conservation makes the pressure first rise above and afterwards drop back below atmospheric pressure.

30.4 Nonlinear surface waves

Linearity is a powerful property because it permits superposition of waves. Any linear wave may in the end be completely resolved into a suitably weighted sum (or integral) over elementary harmonic waves. Leaving the domain of linearity, solutions of this kind are no more possible. Assuming again that the Reynolds number is large, the fields must now satisfy the full nonlinear Euler equation

$$\frac{\partial \boldsymbol{v}}{\partial t} + (\boldsymbol{v}\cdot\boldsymbol{\nabla})\boldsymbol{v} = -\frac{1}{\rho_0}\boldsymbol{\nabla} p + \boldsymbol{g}\ , \qquad \boldsymbol{\nabla}\cdot\boldsymbol{v} = 0\ , \tag{30-44}$$

with $\boldsymbol{g} = (0, 0, -g_0)$. Since there are no general solutions to this equation, nonlinear waves are much more unique and individual than linear waves.

Boundary conditions

The dynamic boundary condition is as before that the pressure must be continuous at the open surface in the absence of surface tension,

$$\boxed{p = p_0 \qquad \text{for } z = h\ ,} \tag{30-45}$$

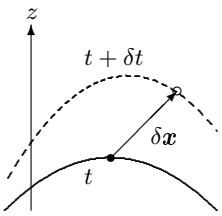

A fluid particle at the surface must follow the motion of the surface from time t to time $t + \delta t$.

The kinematic boundary condition is more complicated, but expresses as before that a fluid particle sitting right at the surface should follow the motion of the surface. In a small interval of time δt, a particle at the surface is shifted by $\delta\boldsymbol{x} = \boldsymbol{v}\delta t$ where $\boldsymbol{v}$ is the velocity field at or rather just below the surface. Since the particle has to remain on the surface, the new height must equal the old plus the vertical shift δz, or

$$h(x + \delta x, y + \delta y, t + \delta t) = h(x, y, t) + \delta z\ .$$

Expanding to first order in the horizontal displacements $\delta x = v_x\delta t$ and $\delta y = v_y\delta t$, and setting $\delta z = v_z\delta t$, we obtain the general kinematic condition,

$$\boxed{\frac{\partial h}{\partial t} + v_x\nabla_x h + v_y\nabla_y h = v_z\ , \qquad \text{for } z = h\ .} \tag{30-46}$$

which may be viewed as a dynamic equation for the wave height. Besides the open surface conditions, there will as for small-amplitude waves be further boundary conditions that depend on the shape of the container.

In the bottomless ocean the only condition is that the influence of surface waves should not penetrate to infinite depth, and as we have seen for small-amplitude waves the influence penetrates in fact only to a depth of about one wavelength. In section 30.6 we shall investigate periodic nonlinear deep-water waves, also called Stokes waves.

At finite depth we may describe the shape of the solid container bottom by its height, $z = b(x, y, t)$, which in the most general case may depend on both

the spatial coordinates and time. The local depth of the fluid is now $d = h - b$. The kinematic bottom condition is obtained in the same way as the open surface condition, and expresses that the fluid must follow the bottom everywhere and at all time,

$$\boxed{\frac{\partial b}{\partial t} + v_x \nabla_x b + v_y \nabla_y b = v_z \ , \qquad \text{for } z = b \ .} \tag{30-47}$$

One should notice that this should not be viewed as a dynamic equation for the bottom height, but rather as a constraint on the flow which is thought to be specified in advance, even if it depends on time. Thus, if the bottom is perfectly flat and horizontal so that b is a constant, this condition degenerates to the usual flat-bottom condition, $v_z = 0$.

* 30.5 The shallow-water approximation

Shallow-water waves are always characterized by being much wider than the depth, $\lambda \gg d$, but in the nonlinear regime the amplitude may be as large as the depth, $a \lesssim d$, although for geometrical reasons it cannot be much larger. Our previous estimate (22-9) shows that the local acceleration in that case will be comparable to the advective acceleration $|\partial \boldsymbol{v}/\partial t| \sim |(\boldsymbol{v} \cdot \boldsymbol{\nabla})\boldsymbol{v}|$. Compared to the gravitational acceleration, the magnitude of the vertical acceleration is estimated to be,

$$\frac{1}{g_0}\left|\frac{\partial v_z}{\partial t}\right| \sim \frac{1}{g_0}\frac{a}{\tau^2} \sim \frac{ad}{\lambda^2} \sim \frac{d^2}{\lambda^2} \ , \tag{30-48}$$

where we have made use of the dispersion law estimate (22-6). In shallow water $\lambda \gg d$ the fluid acceleration is tiny compared to the gravitational acceleration.

Shallow-water equations

Discarding the left hand side of the z-component of the Euler equation (30-44). What is left on the right hand side is the hydrostatic equation $\nabla_z p + \rho_0 g_0 = 0$, and using the dynamic boundary condition (30-45), the pressure becomes,

$$\boxed{p = p_0 + \rho_0 g_0 (h - z) \ .} \tag{30-49}$$

The pressure in a shallow-water wave is always purely hydrostatic. This generalizes the result (22-35d) obtained for small-amplitude shallow-water waves.

In the following we shall for simplicity limit the analysis to line waves in which $v_y = 0$ and all the fields are independent of the y-coordinate, although the formalism for general waves follows along the same lines. Inserting the above pressure solution into the x-component of the Euler equation (30-44) we find

$$\frac{\partial v_x}{\partial t} + (v_x \nabla_x + v_z \nabla_z) v_x = -g_0 \nabla_x h \ .$$

As the right hand side is independent of z, it follows that v_x will be independent of z for all times, if it is so to begin with. We shall from now on assume this to be the case, and putting $v_x = u(x,t)$, the above equation simplifies to

$$\boxed{\frac{\partial u}{\partial t} + \nabla_x \left(g_0 h + \frac{1}{2} u^2 \right) = 0 \ .} \tag{30-50}$$

That the horizontal flow is independent of depth also generalizes the small-amplitude result (22-35b).

The divergence condition becomes $\nabla_z v_z = -\nabla_x u$ and since the right hand side is independent of z, it follows that v_z must be linear in z of the form $v_z = f(x,t) - z\nabla_x u$. This function is determined by imposing the bottom boundary condition (30-47), and we obtain,

$$v_z = \frac{\partial b}{\partial t} + u\nabla_x b + b\nabla_x u - z\nabla_x u \ . \tag{30-51}$$

Inserting this into the kinematic boundary condition (30-46) we arrive at the surprisingly simple dynamic equation for the local depth $d = h - b$,

$$\boxed{\frac{\partial d}{\partial t} + \nabla_x (ud) = 0 \ .} \tag{30-52}$$

Although the coupled partial differential equations (30-50) and (30-52) look formidable enough, they are eminently well suited for numeric integration, given the bottom shape b and initial values for the fields h and u.

Method of characteristics

The shallow-water equations may be partially solved by the so-called *method of characteristics*. As we noted in section 22.1, the phase velocity of long waves is,

$$c = \sqrt{g_0 d} \ , \tag{30-53}$$

which is also the velocity obtained in a free fall from rest through the height d. In a non-linear wave, where $d = d(x,t)$ is a function of both space and time, the local phase velocity also depends on these variables. Eliminating the depth by inserting $d = c^2/g_0$ in the dynamic equations (30-50) and (30-52) and simplifying, we get

$$\begin{aligned} \frac{\partial u}{\partial t} + u\nabla_x u + 2c\nabla_x c &= -g_0 \nabla_x b \ , \\ 2\frac{\partial c}{\partial t} + 2u\nabla_x c + c\nabla_x u &= 0 \ . \end{aligned}$$

Adding and subtracting these equations, they may be written

$$\left(\frac{\partial}{\partial t} + (u+c)\frac{\partial}{\partial x}\right)(u+2c) = -g_0 \nabla_x b \ , \tag{30-54a}$$

$$\left(\frac{\partial}{\partial t} + (u-c)\frac{\partial}{\partial x}\right)(u-2c) = -g_0 \nabla_x b \ . \tag{30-54b}$$

30.6 Nonlinear deep-water gravity waves

Basic formalism

In the nonlinear regime we shall continue to describe surface waves by a height function $z = h(x, y, t)$, although common experience tells us that it may become multivalued when a wave breaks. Assuming again that the Reynolds number is large, so that we may disregard viscosity, the basic dynamic equations are the complete Euler equations (16-1) for incompressible fluid,

$$\frac{\partial \boldsymbol{v}}{\partial t} + (\boldsymbol{v}\cdot\boldsymbol{\nabla})\boldsymbol{v} = -\frac{1}{\rho_0}\boldsymbol{\nabla} p + \boldsymbol{g} \ , \qquad \boldsymbol{\nabla}\cdot\boldsymbol{v} = 0 \ , \tag{30-55}$$

with $\boldsymbol{g} = (0, 0, -g_0)$. Whereas linear waves always can be written as a superposition of an irrotational wave and a constant rotational component, nonlinear waves are not born to be free of vorticity. But, as we saw in section 16.5, a wave that actually is irrotational at any one time, will remain so at all times.

Irrotational nonlinear waves constitute a large — and interesting class — of nonlinear waves for which the velocity field may be derived from a velocity potential

$$\boldsymbol{v} = \boldsymbol{\nabla}\Psi \ , \qquad \boldsymbol{\nabla}^2\Psi = 0 \ . \tag{30-56}$$

In that case the Euler equation may again be solved for the pressure,

$$p = p_0 - \rho_0\left(g_0 z + \frac{1}{2}\boldsymbol{v}^2 + \frac{\partial\Psi}{\partial t}\right) \ , \tag{30-57}$$

which now contains the square of the velocity field (see problem 16.8).

The kinematic boundary condition on the open surface expresses that a fluid particle at the surface should follow the motion of the surface, but as the surface is no more flat it becomes more complicated than (22-16). Consider a fluid particle sitting at the surface which in a small interval of time δt, moves through $\delta\boldsymbol{x} = \boldsymbol{v}\delta t$. Since it has to stay on the surface the vertical change in position δz must equal the change in surface height as we follow the motion, or

$$\delta z = h(x + \delta x, y + \delta y, t + \delta t) - h(x, y, t) \ .$$

Expanding to first order in the displacements and substituting $\delta\boldsymbol{x} = \boldsymbol{v}\,\delta t$, we obtain the general kinematic condition

$$\frac{\partial h}{\partial t} + v_x\frac{\partial h}{\partial x} + v_y\frac{\partial h}{\partial y} = v_z \ , \qquad \text{for } z = h \ . \tag{30-58}$$

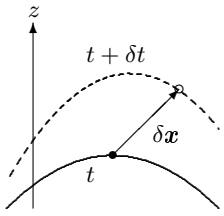

A fluid particle at the surface must follow the motion of the surface from time t to time t + δt.

The dynamic condition is as before that the pressure is continuous at the surface in the absence of surface tension,

$$p = p_0 \qquad \text{for } z = h \ , \tag{30-59}$$

As we have seen, surface tension only affects waves with very short wavelengths and can generally be disregarded in the non-linear regime.

Line waves

Nonlinear gravity waves that are independent of the y-coordinate also form patterns of straight lines along the y-axis and may be called line waves. For such waves, the

Stokes waves

Consider and infinitely deep ocean of infinite horizontal extent interfacing to vacuum (or to a very light fluid) in the absence of surface tension. We shall furthermore limit the discussion to regular parallel trains of (generally non-harmonic) line waves progressing steadily over the surface without changing their shape, a case first analyzed by Stokes in 1847.

Given g_0, such waves are entirely characterized by the wavelength λ and the amplitude a, suitably defined. The only dimensionless quantity which can be constructed from these parameters is the ratio a/λ, or equivalently the *steepness* $ka = 2\pi a/\lambda$. Given the steepness, $\sqrt{g_0 k}$ is the only quantity with dimension of frequency, so that the dispersion law must be of the form,

$$\omega = f(ka)\sqrt{g_0 k} \ , \tag{30-60}$$

where $f(ka)$ is a dimensionless function of the steepness. For $ka = 0$ we must arrive at the linear deep-water expression (22-24), so that $f(0) = 1$.

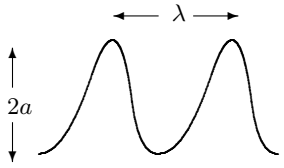

Two periods of a periodic non-linear wave which is not sinusoidal, but nevertheless has a well-defined wavelength, period and amplitude.

The height of a line wave running along the x-axis with constant phase velocity $c = \omega/k$ is a function $h = h(\xi)$ of the variable $\xi = x - ct$, so that $\partial h/\partial t = -c\partial h/\partial \xi$ and $\partial h/\partial x = \partial h/\partial \xi$. This simplifies the kinematic boundary condition to

$$\frac{\partial h}{\partial \xi} = -\frac{v_z}{c - v_x} \ , \tag{30-61}$$

Similarly, the velocity potential may be taken to be of the form $\Psi = \Psi(\xi, z)$. It must be a solution to the Laplace equation, $\nabla_z^2 \Psi = -\nabla_\xi^2 \Psi$, which vanishes for $z \to -\infty$ and is periodic in ξ with period λ. The dynamic boundary condition then becomes,

$$g_0 h = c v_x - \frac{1}{2}\left(v_x^2 + v_z^2\right) + \text{const} \ . \tag{30-62}$$

On the right hand sides of these equations the velocities $v_x = \nabla_\xi \Psi$ and $v_z = \nabla_z \Psi$ must be evaluated for $z = h$. The constant stems from the arbitrariness of Ψ and is chosen such that the average of h vanishes. The solution to these equations determines in principle Ψ, h, and the phase velocity c.

Steepness expansion

Unfortunately, there is no analytic solution, except for $ka \to 0$ where it must approach the linear deep-water solution (22-26). The fact that the linear velocity scale, $a\omega = c\,ka$, is of first order in the steepness $\epsilon = ka$, makes it natural to expand the general solution into powers of this parameter. The phase velocity in powers of ϵ

$$c = \sqrt{\frac{g_0}{k}}(1 + \epsilon C + \epsilon^2 C' + \cdots) \ . \tag{30-63}$$

A further simplification derives from the height being symmetric $h(-\xi) = h(\xi)$ and the velocity potential antisymmetric, $\Psi(-\xi, z) = -\Psi(\xi, z)$, in the small-amplitude limit. Since the nonlinear boundary conditions do not break these symmetries, we may assume that the general solution also has this property.

A symmetric height function with period $\lambda = 2\pi/k$ may always be expanded into a Fourier series of symmetric harmonics $\cos nkx$. Scaling out a dimensional factor a, we may write

$$h = a(A\cos k\xi + \epsilon A' \cos 2k\xi + \epsilon^2 A_3 \cos 3k\xi + \cdots) \ . \tag{30-64}$$

The expansion coefficients A_n are all dimensionless and can thus only depend on the steepness $\epsilon = ka$. We have also factored out ϵ^{n-1} to make each coefficient of order unity (to be confirmed by the explicit solution), and to make contact with the linear case we take $A = 1$.

An antisymmetric velocity potential may similarly be resolved into a Fourier series of antisymmetric harmonics of the form $e^{nkz}\sin nk\xi$, with an exponential term needed to satisfy the Laplace equation. Scaling out a dimensional factor ac we may write,

$$\Psi = ac\left(B_1 e^{kz}\sin k\xi + \epsilon B' e^{2kz}\sin 2k\xi + \epsilon^2 B_3 e^{3kz}\sin 3k\xi + \cdots\right) \ , \tag{30-65}$$

where the expansion coefficients B_n are all dimensionless and of order unity.

Problems

30.1 Show that the linear approximation in (30-8) is better than 3.3% for $\mathsf{Fr} > 2$.

30.2 Investigate mass conservation for the river bore and the reflection bore.

30.3 Verify that the solution of the Rankine-Hugoniot relations (30-19) is

$$U' = \frac{\gamma - 1}{\gamma + 1} U + \frac{2\gamma}{\gamma + 1} \frac{p}{\rho U} \ , \tag{30-66a}$$

$$\frac{1}{\rho'} = \frac{\gamma - 1}{\gamma + 1} \frac{1}{\rho} + \frac{2\gamma}{\gamma + 1} \frac{p}{\rho^2 U^2} \ , \tag{30-66b}$$

$$p' = -\frac{\gamma - 1}{\gamma + 1} p + \frac{2}{\gamma + 1} \rho U^2 \ . \tag{30-66c}$$

30.4 Show that the entropy change (30-24) is a growing function of σ for $\sigma > -1$.

